Influence of neighbouring damage on delamination growth in multiple indented composites

Huo, L.; Kassapoglou, C.; Alderliesten, R.C.

DOI
10.1016/j.matdes.2023.111723

Publication date
2023

Document Version
Final published version

Published in
Materials & Design

Materials & Design 227 (2023) 111723

Contents lists available at ScienceDirect

Materials & Design

journal homepage: www.elsevier.com/locate/matdes

Influence of neighbouring damage on delamination growth in multiple indented composites

L. Huo *, C. Kassapoglou, R.C. Alderliesten

Faculty of Aerospace Engineering, Delft University of Technology, P.O. Box 5058, 2600 GB Delft, The Netherlands

HIGHLIGHTS

- The effect of the neighbouring pre-existing damage on delamination growth is quantified using a proposed stress-based delamination growth prediction method.
- The stress field is determined using a finite element model, and damages are detected and quantified through ultrasonic scanning and optical microscopy.
- The delamination that occurs second in the multiple-indented composite laminate is more likely to propagate at the ply interface.
- The more easily propagated delamination could result from a degradation of the delamination growth threshold caused by the presence of the neighbouring damage.

GRAPHICAL ABSTRACT

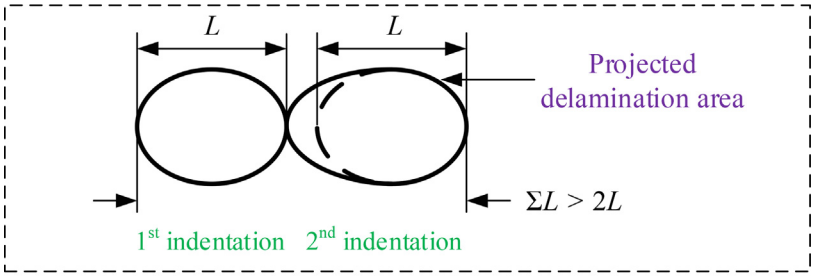

Neighbouring damage effects cause a larger projected delamination area than the sum of two identical out-of-plane quasi-static indentation cases.

ARTICLE INFO

Article history:
Received 21 October 2022
Revised 9 February 2023
Accepted 9 February 2023
Available online 11 February 2023

Keywords:
Polymer-matrix composites
Quasi-static indentation
Delamination growth
Delamination link-up

ABSTRACT

To improve current design approaches for composite structures, it is required to further investigate the damage interaction effects of composite materials under multiple out-of-plane concentrated loads. It is first necessary to comprehend the dependence of the effective delamination threshold, which describes whether a delamination grows on pre-existing delamination damage in composite laminates. A combined experimental and numerical study is presented, in which two sequential out-of-plane quasi-static indentations are applied to fully clamped composite laminated panels, with changing distances between the two indentation locations changing. The results show that the second indentation delamination is more likely to propagate, particularly in the straight-line direction from the second indentation site to the first one, which can be interpreted as a decrease in the effective delamination threshold associated with microcracks ahead of the delamination front. The relevant percentage reduction is 37% and is independent of the imposed indentation load. As a crucial take-away, designers should be mindful that the damage interaction effects could result in greater damage than the sum of the individual cases.

1. Introduction

Fibre-reinforced polymer composite (FRP) laminates are widely used in aviation structures, primarily due to their high

* Corresponding author.
E-mail address: L.Huo@tudelft.nl (L. Huo).

https://doi.org/10.1016/j.matdes.2023.111723
0264-1275/

strength-to-mass and stiffness-to-mass ratios [1], which have attracted interest of numerous researchers [2–5]. However, owing to their weak through-thickness strength, FRP laminates are susceptible to out-of-plane concentrated loads, which often occur during quasi-static indentation [6], low-velocity impacts [7], and high-velocity impacts [8]. Delamination, matrix cracking, and fibre breakage are the three main damage modes of FRP laminates under these loading conditions [9]. Those induced damages usually have detrimental effects on the fundamental properties of composite laminates, causing stiffness and strength degradation [10,11].

Over the past several decades, many studies have focused on the damage behaviour associated with single impacts or indentations applied to FRP composite laminates [12–16]. Through these studies, the damage resistance and tolerance of diverse composite laminates with distinct geometric features and mechanical properties have been compared. However, concerns may arise regarding whether this particular single loading condition is representative of actual loading conditions that a composite structure encounters throughout its service life. Impact events such as hail impacts, generally occur randomly and multiple times on the exposed surfaces of composite structures [17].

To address this concern, several studies have considered a more representative loading condition: two single impacts at separate sites on composite laminates [18–20]. Zhou et al. [18] characterised the similarities and differences between the first and second impacts by comparing the force–time curves, force–displacement curves, velocity–time curves, and energy–time curves. Liao et al. [19,20] used the same method in their investigations. These studies focused mostly on comparing the macroscopic quantities resulting from the first and second impacts; damage characteristics such as matrix cracking, delamination, and fibre breakage of the first and second impacts were not investigated in detail. In fact, if two single impacts do not occur simultaneously, the pre-existing damages induced by the first impact may affect the formation of the second impact damages. Quantification of potential damage influences by sudden or apparent slope variations in the impact curves (e.g. load drop in the force–displacement curve) is inconclusive as the relationship between damage formation and changes in the impact curves is not well understood [21–25]. Alternatively, more directly related metrics such as the increase or decrease in the effective damage initiation and propagation thresholds can be used to quantify the effects of the first impact damage on the formation of the second impact damage.

To this end, a combined experimental and numerical investigation was conducted on the delamination formation response of CFRP composite laminates with fully clamped boundary conditions subjected to multiple quasi-static indentations. These consist of two out-of-plane quasi-static indentations with identical loading rates, peak indentation forces, and indenter geometries were successively applied to separate sites on the front surfaces of composite laminates. Ultrasonic C-scanning and optical microscopy were used to obtain damage information for the composite specimens. Finite element (FE) analyses in ABAQUS, which incorporated material property degradation induced by matrix cracks and fibre failure, were used to determine the indentation stress fields.

The selection of quasi-static indentation over impact loading was prompted by the desire to prevent additional noise caused by the dynamic response of the device and coupons during low-velocity impact testing. In addition, with indentation as a baseline, dynamic effects can be studied later by correlating the results from impact testing with the indentation results. Several studies have been conducted on the relationship between quasi-static and dynamic indentations on composites [25–28]. More important, the quasi-static indentation test offers an advantage over the dynamic impact test in terms of better control of the exact loading location, which is essential for investigating multiple indentations at distinct locations with precise distances.

2. Effects of existing damage on subsequent damage creation

In general, strength is defined as the ability of a material to withstand failure. At the length scale of the ply thickness, the strength of unidirectional FRP composite laminates is a function of the fibre orientation, loading type, and differences between the in-plane and out-of-plane properties. Many studies have evaluated the degree of strength degradation of FRP composite laminates as a function of the type and extent of damage by calculating the residual compressive, tensile, and flexural strengths [14,29–34]; the term *damage tolerance* is used to describe the performance of composites with various damages [7]. Owing to the complexity of the flexural stress field in the presence of damage [7], the relationship between specific damage modes and their degradation in flexural strength remains unclear despite the fact that several relevant studies [35–37] have been conducted.

Furthermore, the effective thresholds for damage initiation and propagation are correlated with the strength of FRP composite laminates. In this scenario, the effective damage thresholds for an FRP laminate are the effective matrix crack initiation threshold, effective fibre failure threshold (compressive or tensile strength of the fibre), and effective delamination propagation threshold. Thus, existing damage not only defines how damage propagates under load, but may also affect the creation, type, and size of externally imposed damage in its vicinity (e.g. by impact). In other words, impact damage in a pristine structure may be different from impact damage in the same structure with pre-existing damage.

The purpose of this study is to determine whether the influence of the first-indentation damages on the propagation of the second-indentation delaminations can be evaluated by examining the effect of the first-indentation damage on the effective second-indentation delamination thresholds. As damage generally results with material strength degradation, the effective second-indentation delamination thresholds are expected to degrade when there are pre-existing damages in the vicinity of the second indentation delamination front.

To aid this study, a delamination prediction method proposed by the authors in a previous study [38] is used to assess the reduction in the effective propagation threshold of a newly formed delamination as a result of pre-existing damage. With this approach, the potential interactions between adjacent damage locations can be studied, and a framework for studying the effect of multiple adjacent damage locations can be created.

3. Overview of method for predicting delamination

3.1. Delamination growth criterion

In a recent study by the authors [38], a concise Hashin-type delamination propagation criterion was developed to predict delamination growth along the fibre orientations to singly indented CFRP laminates. The equation for the criterion for delamination growth is

$$\left(\frac{\sigma_{13}}{S_{13}}\right)^2 = 1 \tag{1}$$

where σ_{13} is the local transverse shear stress at the ply interface; the 1-axis is parallel to the fibre orientation of the lower ply (ply further away from the indentation site) of the considered ply interface, and the 3-axis is aligned with the z-axis depicted in Fig. 1. S_{13} is the out-of-plane (interlaminar) shear strength of the correspond-

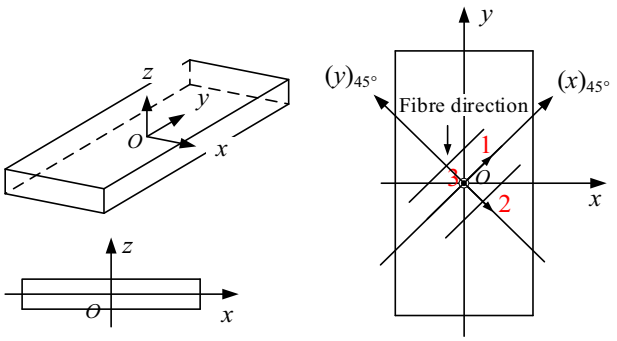

Fig. 1. Cartesian coordinate systems: global coordinate systems (black *x*-*y*-*z* and $(x)_{45°}$-$(y)_{45°}$-*z*) and local coordinate system (red 1-2-3). (For interpretation of the references to colour in this figure legend, the reader is referred to the web version of this article.)

ing unidirectional laminate made from M30SC/DT120 prepreg (Table 1).

Eq. (1) shows that along the lower ply fibre direction, delamination grows when the out-of-plane shear stress σ_{13} is greater than the out-of-plane shear strength S_{13}. In this context, the out-of-plane shear strength can be considered the effective delamination growth threshold in the considered direction. Consequently, changes in this delamination growth threshold value can be used to assess the influence of pre-existing damage on the propagation of subsequent adjacent damage.

3.2. Description of FE model

Clearly, the accuracy of the indentation stress field is critical for predicting the delamination growth using the proposed criterion. To determine the indentation stress field of the single-indented CFRP laminates, as shown in Fig. 2, an M30SC/DT120 carbon/epoxy composite laminate with layup $[45/0/-45/90]_{2s}$ and dimensions of 150 mm × 300 mm × 2.5 mm was modelled. The material property parameters used in the FE model were obtained from material data sheets [39,40] and were shown in [38,41] to be sufficiently accurate for the purposes of this investigation. For convenience, they are summarised in Tables 1 and 2. To improve the simulation accuracy, geometric nonlinearity was considered, and the 25-mm-diameter steel hemispherical indenter was assumed to be a rigid body. The contact between the indenter and plate was modelled as the surface-to-surface type in which the normal behaviour was treated as 'Hard' and tangential behaviour was characterised using the penalty method with a friction coefficient of 0.3 [38]. A sensitivity investigation that changed the friction coefficient from 0.2 to 0.4 indicated no significant differences in the force–deflection curves of the simulated laminates.

Table 1
Unidirectional laminate strengths of M30SC/DT120 (quasi-static loading condition) [39].

Strength	Test standard	Test result [MPa]
X_T	ASTM D 3039	3010
X_C	ASTM D 6641	1020
Y_T	ASTM D 3039	39
Y_C	ASTM D 6641	138.0
Z_T	–	39
S_{12}	EN 6031	95.6
S_{13} (S_{23})	EN 2563	77.2

Note: Z_T is estimated based on Y_T, the 1-direction is parallel to the fibre direction, the 2-direction is in-plane and normal to the fibre direction, and the 3-direction is parallel to the out-of-plane direction, S_{ij} (i = 1, 2, 3; j = 1, 2, 3, $i \neq j$) are the shear strength parameters, *X* is the strength parallel to the fibre direction, *Y* and *Z* are the strengths normal to the fibre direction with *Z* out-of-plane, C and T refer to compressive and tensile, respectively.

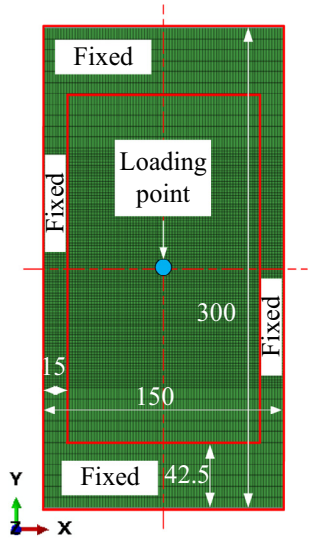

Fig. 2. Details of the FE model used to predict single-indentation stress field [38].

Table 2
Elastic material properties for M30SC/DT120 prepreg [40].

Density	ρ = 1.76 g/cm^3
Young's modulus of material	E_{11} = 155 GPa, E_{22} = E_{33} = 7.8 GPa, G_{12} = G_{13} = 5.5 GPa, G_{23} = 3.25 GPa*
Poisson's ratio	υ_{12} = υ_{13} = 0.27, υ_{23} = 0.2*

* G_{23} is estimated, and υ_{23} is calculated by assuming that the 2–3 plane is isotropic.

In addition, each layer had a thickness of 0.15 mm and was meshed using C3D8I (8-node linear brick, incompatible elements) to address any potential convergence issues. All degrees of freedom of the corresponding regions whose inner boundaries were within 15 mm and 42.5 mm from the numerical plate edges were constrained (Fig. 2); these regions are denoted as 'fixed'. Lastly, this model accounted for damage-induced mechanical property degradation by incorporating the Puck failure criteria [42] and the constant stress exposure (CSE) progressive stiffness degradation technique [43]. The delamination and its effect on the indentation stress field distribution were not considered; this simplification was supported by the results. The FE model can accurately predict the indentation stress field of the indented composite laminates, as shown in [38], because of the good agreement between the predicted and experimentally measured delamination sizes.

3.3. Determination of delamination length

The delamination length in the direction of the fibres is defined as the maximum length of all single delaminations at different ply interfaces:

$$L_\Theta = \max\{l_{\Theta 1}, l_{\Theta 2}, \cdots, l_{\Theta n}\},\ \Theta = \ 0^\circ, 45^\circ, 90^\circ, -45^\circ\} \quad (2)$$

where $l_{\Theta n}$ is the maximum delamination length at the n^{th} ply interface (the first one is closest to the indented surface) along the fibre direction Θ. To demonstrate the determination of delamination lengths using this concept, the determination of length $L_{45°}$ for a composite laminate under an indentation force of 3000 N is illustrated in Fig. 3. Note that $L_{45°} = l_{45°11}$ in this case indicates that

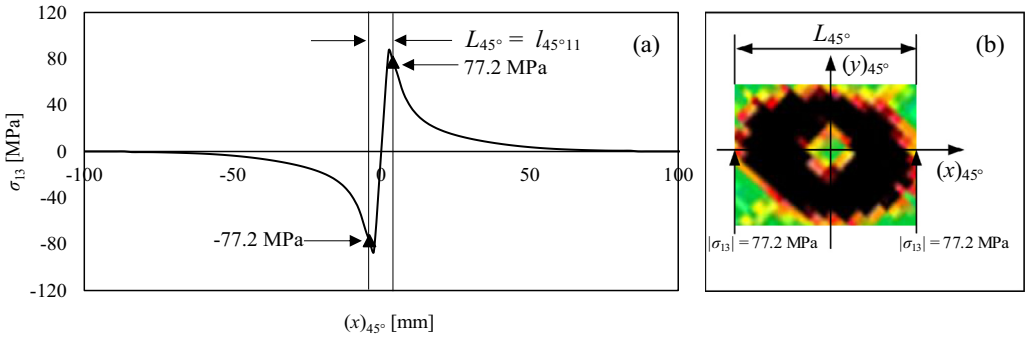

Fig. 3. Determination of delamination length $L_{45°}$: (a) shear stress distribution on eleventh ply interface determined by the FE model; the single delamination length in the 45° fibre direction has the maximum value at the eleventh interface [38]; (b) definition of $L_{45°}$ of the C-scan projected delamination area; the coordinate system is shown in Fig. 1.

the eleventh ply interface delamination length is the maximum in the 45° direction [38].

As shown in Fig. 3(a), the value of the delamination length $l_{45°11}$ is equal to the distance between the points on the out-of-plane shear stress profile, whose absolute values are equal to the interlaminar shear strength (S_{13}), covering the region in which the shear stress exceeds its ultimate strength value. As the eleventh ply interface delamination has the maximum value in the 45° fibre direction [38], the projected delamination length $L_{45°}$ is taken as the value of $l_{45°11}$. Two additional stress points with the same absolute value as the interlaminar shear strength can be noticed between the minimum and maximum stress points of the shear stress profiles. During the static indentation, delamination cannot propagate in that region, as the out-of-plane compression stress induced during the indentation process prevents delamination from propagating.

4. Experimental details

4.1. Material and test fixture

For consistency with an earlier study [38], the CFRP panels were fabricated with the same hand lay-up process using the unidirectional carbon/epoxy prepreg M30SC/DT120 supplied by Delta-Tech S. p. a. The CFRP panels were placed in an autoclave and cured for 90 min at 120 ℃ and a pressure of 6 bar. The resulting panels were cut with a diamond saw into rectangular specimens with dimensions of 150 mm × 300 mm and a nominal thickness of 2.5 mm, consistent with the FE model (Fig. 2). The specimens had a quasi-isotropic layup $[45/0/-45/90]_{2s}$ in which the 0° fibre direction was aligned with the short edges (the x-axis direction, as shown in Fig. 1). Prior to testing, all specimens were ultrasonically C-scanned; only those free of flaws were used in the tests.

In this study, a test fixture with a 120 mm × 215 mm rectangular window was used, as shown in Fig. 4(a). Using this fixture, the short edges of the specimen were fastened with bolts that passed through it, and the two long edges were clamped by the contact pressure. As this study considers two identical indentations applied at separate locations and investigates the effect of damage associated with the first indentation on the formation of the second indentation delaminations, the two indentations must be applied to regions with similar damage behaviours. To ensure that only the first indentation damages directly or indirectly influence the formation of the second indentation delaminations, the factors (primarily the target plate geometry effect [24]) that could potentially influence the damage behaviour should remain the same whenever a single indentation is applied to these regions. According to a previous study by Huo et al. [41] on composite laminates subjected to eccentric indentations, using the test fixture depicted in Fig. 4(a), the multiple indentations should be applied to the circular central region of the specimen with a diameter of at least 30 mm.

4.2. Multiple quasi-static indentation test

The multiple quasi-static indentation tests were performed using a Zwick Roell 20-kN servo-hydraulic test machine, as illustrated in Fig. 4(b). The out-of-plane indentations were applied vertically on the front surfaces of the specimens at a constant indentation rate of 15 mm/min using a steel hemispherical indenter with a diameter of 25 mm, in accordance with the indentation plan depicted in Fig. 4(c). The two loading points were antisymmetric about the centrelines of the specimen (the x- and y-axes, as illustrated in Fig. 1). The first indentation position was I_1, followed by I_2; each site was indented once. The primary objective of such an indentation arrangement is to maximise the use of space on the specimens with similar single indentation damage behaviours. The indentation tests were conducted under displacement control, with each indentation applied up to a predefined indentation force before the indented specimens were unloaded. In this study, the predefined indentation forces for the specimens were 3000 N, 4000 N, and 5000 N. The summary of these test details is shown in Table 3.

4.3. Damage detection

After conducting the quasi-static indentation tests, ultrasonic C-scanning was performed to determine the projected delamination areas. The specimens were ultrasonically C-scanned using a through-transmission method: the coaxial cylindrical acoustic wave transmitter and receiver were mounted on opposite sides of the composite specimen immersed in water. OLYMPUS supplied the transmitter and receiver, which were both designated as V311-SU. The ultrasonic inspection settings were configured using an OLYMPUS EPOCH 650 digital ultrasonic flaw detector. To automate the damage detection, the software NI LabVIEW 2018 SP1 was employed for the stepper motor driver control, data acquisition, and imaging. The chosen speed for the direct vertical axis was 200 mm/s, whereas the speed for the direct horizontal axis was 1 mm/s. Subsequently, one specimen from each test group (Table 3) was sectioned along the red line, as shown in Fig. 4(c), and the exposed cross-sections were progressively ground using sandpaper with grain sizes of 82 μm, 46.2 μm, 18 μm, 8 μm, and 5 μm. After that, diamond pastes were used to polish each sample. Lastly, the cross-sectional damage micrographs were obtained using a Keyence VK-X3000 microscope at 5× and 15× magnifications and then

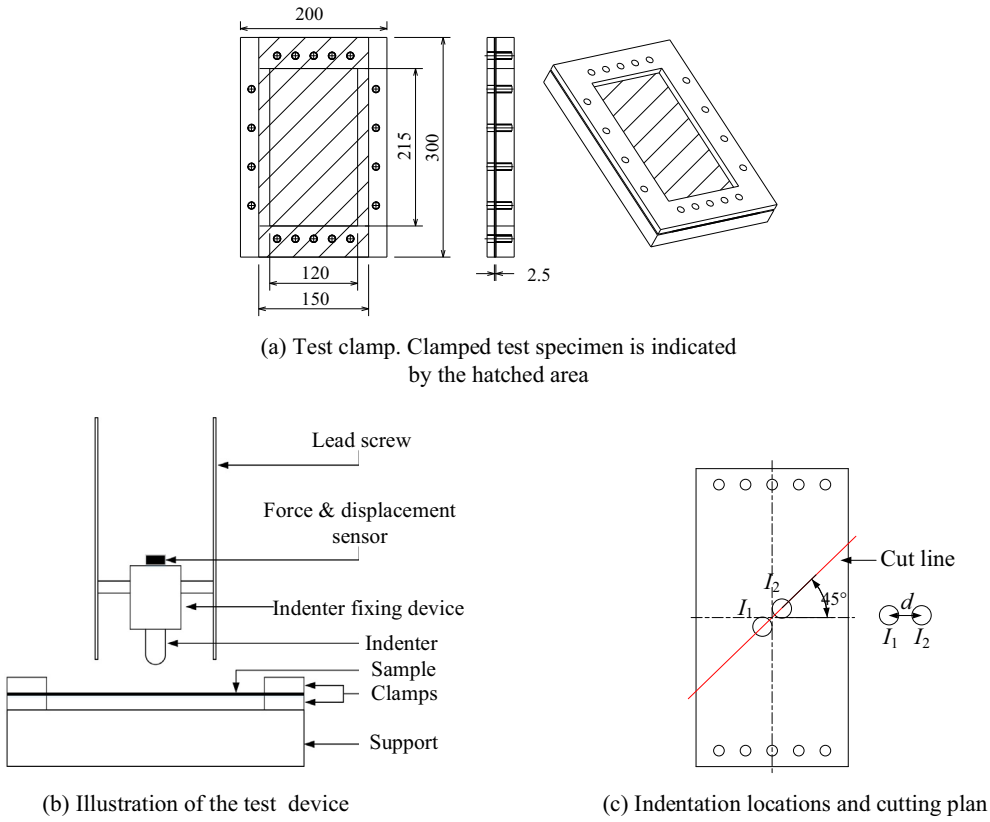

(a) Test clamp. Clamped test specimen is indicated by the hatched area

(b) Illustration of the test device

(c) Indentation locations and cutting plan

Fig. 4. Overview of multiple quasi-static indentation test and ultrasonic C-scan equipment.

Table 3
Test matrix.

Test group	Number of coupons	Predefined indentation force [N]	d [mm]
QSI_01	3	5000	5
QSI_02	3	5000	12
QSI_03	3	5000	17
QSI_04	3	5000	22
QSI_05	3	5000	27
QSI_06	3	3000	12
QSI_07	3	4000	17

post-processed using AutoCAD 2021 software for illustration purposes.

5. Results and discussion

In this section, the C-scan damage recordings for the multiple-indented composite laminates under an indentation force of 5000 N and different loading distances were used to illustrate the delamination link-up effects. Subsequently, the delamination link-up effects were investigated using the proposed method presented in Section 3. Finally, the conditions for generalising this study are discussed along with some limitations.

5.1. Characteristics of multiple indentation damages and assessment of delamination interaction

C-scan records of the specimens with two successive identical indentations were used to examine the possible interactions. The C-scan results of the specimens indented with an identical peak force of 5000 N and loading distances (d) ranging from 5 mm to 27 mm are presented to highlight the typical characteristics of all multiple indentation damages. The C-scan results are given in Fig. 5, using the coordinate system shown in Fig. 1.

As shown in Fig. 5, the link-up of the two projected delamination areas of both indentations is of particular significance. Beyond d > 22 mm, these two single delamination areas were no longer connected, as shown by the two separate C-scan damages (Fig. 5 (e)). Consequently, the loading distance d = 22 mm is an approximation of the critical distance for the delamination area link-up, indicated in this study as d_{crit}. Note that, based on the accuracy of the C-scan equipment, which has been determined to be on the order of 1–2 mm for normal damage sizes, the exact critical distance is likely greater than 22 mm.

Thus, the two delamination areas merged at approximately d = 22 mm. The question is whether the merging of delamination areas is simply the superposition of two distinct delamination areas or whether actual link-up effects occur, that is, whether the second indentation delamination area is affected by the existence of the first one. To determine whether delamination areas merely merge or whether actual link-up effects occur, the C-scan results were analysed following the concept presented in Fig. 6. In Fig. 6, ΣL refers to the maximum length of the connected projected delamination areas along the 45° direction if $d \leq d_{crit}$; otherwise, ΣL is simply the sum of the major axis lengths of the two isolated oval delamination areas.

The delamination areas shown in Fig. 5 were quantified and plotted in Fig. 7, where Eq. (3) defines how the two delaminations merge without link-up effects. If there are no interactions between the first and second indentation delamination areas, as shown in Fig. 5, ΣL should be a simple superposition of the corresponding single delamination length $L_{45°}$; in this instance, $(L_{45°})_1$ =

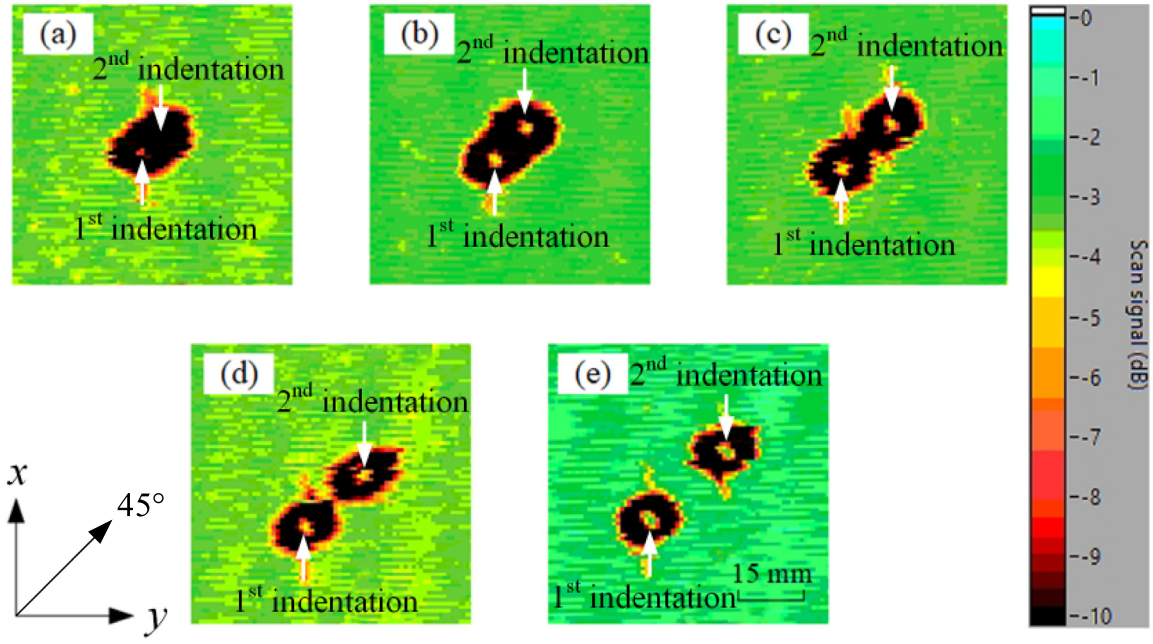

Fig. 5. Ultrasonic C-scan damage morphologies of the specimens subjected to two consecutive indentations with an identical indentation force of 5000 N and different loading distances: (a) d = 5 mm; (b) d = 12 mm; (c) d = 17 mm; (d) d = 22 mm; (e) d = 27 mm.

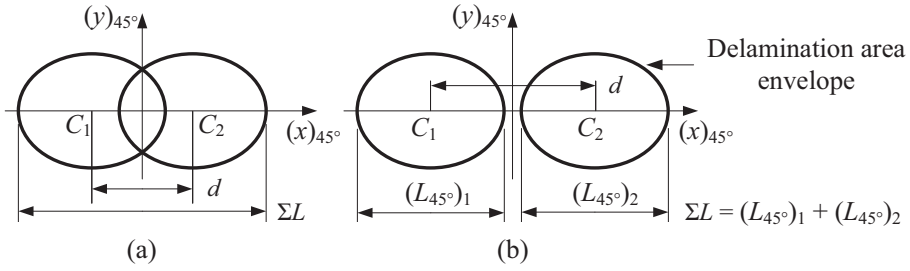

Fig. 6. Definition of ΣL for the loading cases: (a) $d \le d_{crit}$ and (b) $d > d_{crit}$, where $(L_{45^\circ})_1$ and $(L_{45^\circ})_2$ are the isolated delamination lengths of the first and second indentations in the 45° direction, respectively; the associated coordinate system is depicted in Fig. 1.

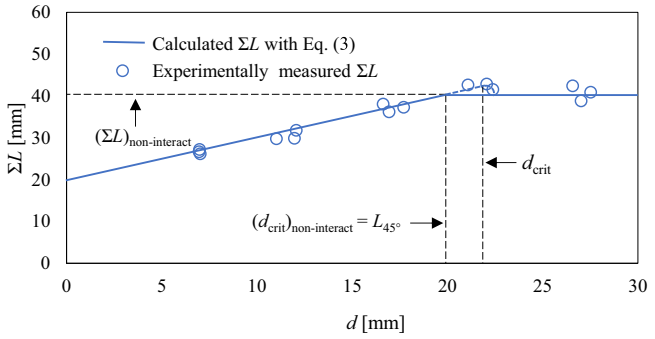

Fig. 7. Comparison of the calculated and experimentally measured ΣL; the indentation force was 5000 N. $(d_{crit})_{non\text{-}interact}$ refers to the critical loading distance for delamination area link-up without potential link-up effects. The C-scan device accuracy is on the order of 1–2 mm for typical damage sizes.

$(L_{45^\circ})_2 = L_{45^\circ}$. The delamination superposition implies a linear increase from L_{45° to $2L_{45^\circ}$ at link-up, with a value of $2L_{45^\circ}$ beyond that point.

$$\sum L = \begin{cases} d + L_{45^\circ} & d \leqslant L_{45^\circ}; \\ 2L_{45^\circ} & d > L_{45^\circ}. \end{cases} \quad (3)$$

The single delamination length, which was measured from the C-scan record and used to calculate ΣL, was obtained from a previous study [38] by the authors.

As the specimens were C-scanned using the same equipment with the same settings, the errors should be comparable for different C-scan results (the C-scan machine accuracy is on the order of 1–2 mm for typical damage sizes). Thus, the discrepancy between the data and the curve shown in Fig. 7 illustrates the possibility of link-up effects. The variation of ΣL with d is linear between $(d_{crit})_{non\text{-}interact}$ and d_{crit}, which is easily understood by altering the definition of ΣL in Eq. (3) with $d \le L_{45^\circ}$ replaced by $d \le d_{crit}$. In addition, ΣL attains its maximum value at the critical loading distance. However, without further investigation, it is unclear exactly how ΣL precisely changes immediately after d_{crit} is reached. In fact, the damage interaction is also present even when the two delamination areas are no longer connected. This causes ΣL to reach its maximum value at $d = d_{crit}$ and then gradually return to $(\Sigma L)_{non\text{-}interact}$ = 40 mm (Fig. 7).

The C-scan records are two-dimensional, showing only an envelope image of the outer borders of multiple delaminations. Thus, cross-sectional damage analysis was used to actually demonstrate the essence of the delamination area link-up. The cross-sectional damage morphologies of the specimens sectioned along the path shown in Fig. 4(c) are illustrated in Fig. 8. It can be seen

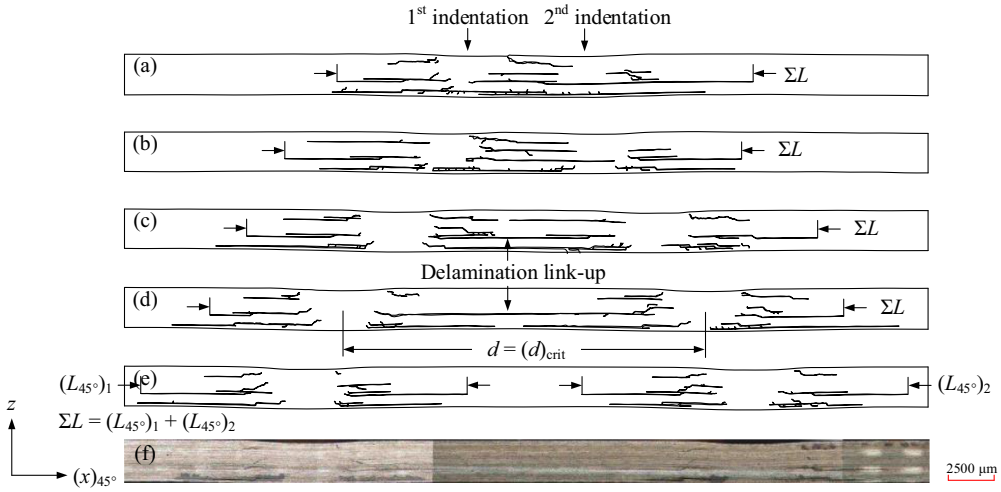

Fig. 8. Cross-sectional damage morphologies of the specimens subjected to two successive indentations with identical indentation force of 5000 N and different loading distances: (a) d = 5 mm; (b) d = 12 mm; (c) d = 17 mm; (d) d = 22 mm; (e) d = 27 mm; (f) the original damage micrograph of case (e). The definition of ΣL is in terms of delamination length, where $(L_{45^\circ})_1$ and $(L_{45^\circ})_2$ refer to the isolated delamination lengths of the first and second indentations in the 45° direction. The left and right indentations in (b) – (e) refer to the first and second indentations, respectively, as in (a).

from Fig. 8 that the delamination area link-up shown in Fig. 5 is essentially the connection, at the same single interface, of delaminations emanating from two different indentation sites and propagating from opposite directions. The delaminations at the eleventh ply interface of the multiple-indented laminates are generally the largest; and ΣL can be represented by the lengths of the longest delaminations ($d \leq d_{crit}$) or the sum of the two isolated delamination lengths ($d > d_{crit}$).

Note that the stress profile during the second indentation yielded low stresses in the area of the first indentation delamination. Thus, the link-up constituted only the extra growth of the second indentation delamination, as illustrated in Fig. 9. The underlying cause for this added growth in the second indentation could be interpreted as a reduction in the effective delamination threshold.

5.2. Prediction of critical loading distance for delamination link-up

Using the prediction model described in Section 3 to predict both the first and second indentations would yield identical delaminations, as if the damage interaction effects were not considered. To predict a longer delamination length with the critical loading distance, the delamination criterion in Eq. (1) suggests that either the stress is higher or that the effective threshold strength decreases. In the critical case, $\Sigma L = d_{crit} + L_{45}$, where $L_{45^\circ} = l_{45^\circ 11}$ and is the sum of the semi-major lengths of the delamination areas next to the regions A and C (Fig. 9), and is not influenced by the link-up effect. Therefore, in this case, the prediction of ΣL is essentially equivalent to predicting d_{crit}.

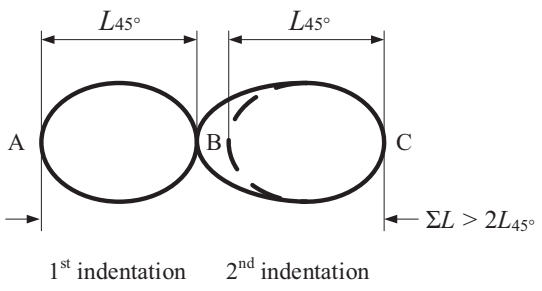

Fig. 9. Illustration of the extra second indentation delamination growth influenced by the link-up effects.

5.2.1. Similarity between out-of-plane shear stress profiles of second indentations with and without first indentation damages

By adjusting the indentation locations accordingly, the first and second indentation out-of-plane shear stress profiles were determined using the calibrated FE model. The peak stresses associated with the delamination link-up can be compared with the pristine interlaminar shear strength of the material. To substantiate the validity of the FE model in predicting the second indentation deformation behaviour from the first indentation damages was first demonstrated by the good agreement between the experimental and simulation force–displacement curves (Fig. 10). The indentation force was 5000 N with $d = d_{crit}$ = 22 mm and d = 27 mm. The excellent curve matching suggests that the major features of the global second indentation stress field distribution can be captured by this FE model [38].

Subsequently, the eleventh-ply interface numerical stress profiles for the first and second indentations were obtained, as shown in Fig. 11. The second indentation stress profiles were separately predicted with and without the first indentation matrix cracking and fibre breakage damages to highlight the stress distribution anomalies (indicated by the red arrows in Fig. 11). To accomplish

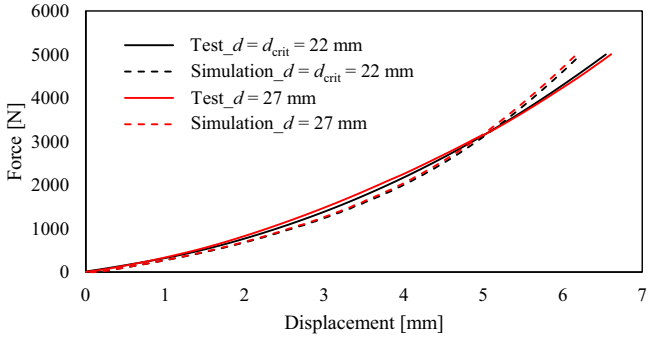

Fig. 10. Comparison of loading phase of the second indentation force–displacement curves predicted by the FE model with first indentation damages and those obtained from the test, with an indentation force of 5000 N.

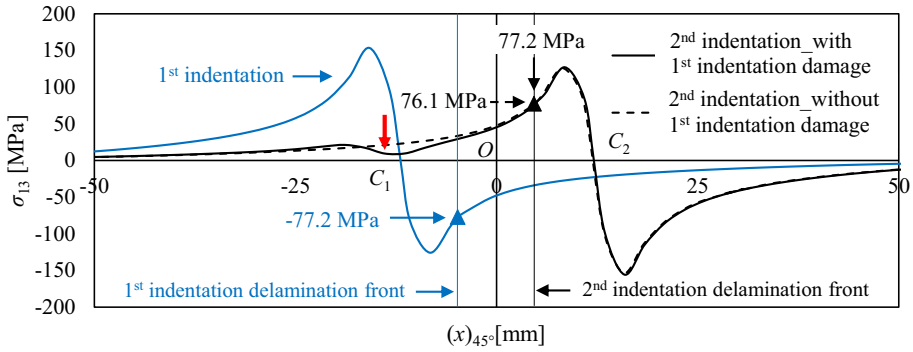

(a) $d = 27$ mm, i.e., $|C_1C_2| = 27$ mm

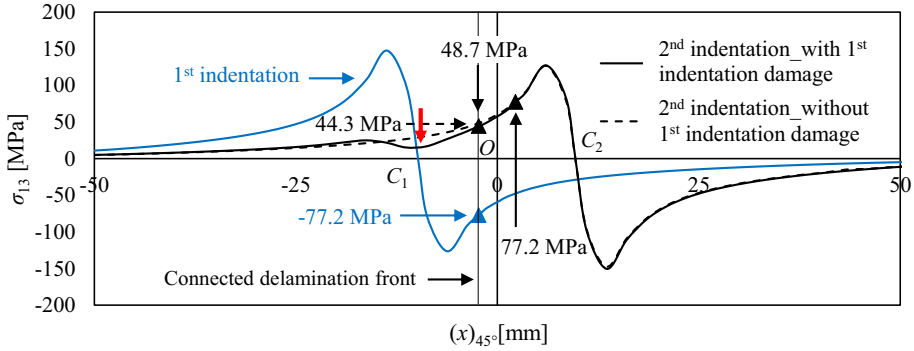

(b) $d = d_{crit} = 22$ mm, i.e., $|C_1C_2| = 22$ mm

Fig. 11. Out-of-plane shear stress profiles of the first and second indentations along the delamination link-up direction at the eleventh-ply interface with an indentation force of 5000 N; the associated coordinate system is shown in Fig. 1. The red arrow indicates the stress profile anomaly caused by the first indentation damages (matrix cracking and fibre breakage), and note that without damage interaction, the first and second indentation stress profiles are symmetrical about the original point *O*. (For interpretation of the references to colour in this figure legend, the reader is referred to the web version of this article.)

this, two consecutive indentations were simulated with and without the UMAT subroutine.

The simulation results (Fig. 11) revealed that, for both cases, such stress profile anomalies were restricted to the first indentation centre regions, whereas the second indentation delamination front shear stresses were only marginally affected. More specifically, the absolute stress values of the second indentation delamination fronts for d = 27 mm with and without the first indentation damages (Fig. 11(a)) were 77.2 MPa and 76.1 MPa, respectively; their $d = d_{crit}$ = 22 mm counterparts were 48.7 MPa and 44.3 MPa (Fig. 11 (b)). In particular, the simulation results for the critical case showed only marginal changes in the stress profiles due to the pre-existing damages, whereas a lower stress value was found at the second delamination front, such that the value of $|C_1C_2|$ was equal to d_{crit} (Fig. 11(b)).

As the indentation force steadily increased from 0 N to 5000 N in the second indentation, the eleventh ply interface delamination progressively propagated toward the first indentation site until link-up. At the point where the delaminations were just connected, the absolute stress of the second indentation delamination front can be regarded as the effective delamination growth threshold, which was 48.7 MPa, as illustrated in Fig. 11(b). This indicates that the effective second delamination growth threshold decreased from 77.2 MPa to 48.7 MPa (~37 % decrease from its initial value), providing a possible explanation for the gap between the calculated and measured ΣL at the critical distance in Fig. 7.

5.2.2. Development of delamination growth criterion

As the effective second indentation stress profile at the eleventh ply interface was minimally affected by the first indentation damages for $d = d_{crit}$, the second indentation stress profile without the pre-existing damages was used to determine the delamination size. Consequently, the second indentation stress profile can be determined via the origin symmetry relationship with the first indentation stress profile, with a significant increase in computing efficiency.

With an effective delamination threshold of 77.2 MPa, the second delamination did not link with the first one; to explain the test results, the effective delamination growth threshold must be reduced from 77.2 MPa to 48.7 MPa (Fig. 11(b)). Therefore, at an indentation force of 5000 N, the criterion for predicting the growth of the second indentation eleventh ply interface delamination in the critical case is:

$$\left(\frac{\sigma_{13}}{\zeta S_{13}}\right)^2_{5000N,\ 11th} = 1,\ \zeta = 0.63 \tag{4}$$

where ζ is the effective reduction factor, which was deduced by combining the test results with the finite element simulation.

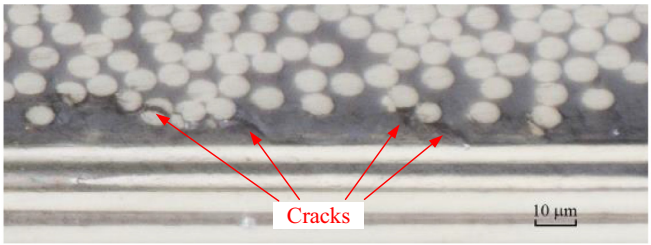

Fig. 12. Microcracks at the delamination front observed at the fifth ply interface of the specimen with an indentation force of 5000 N, and to the right end relative to the indentation centre.

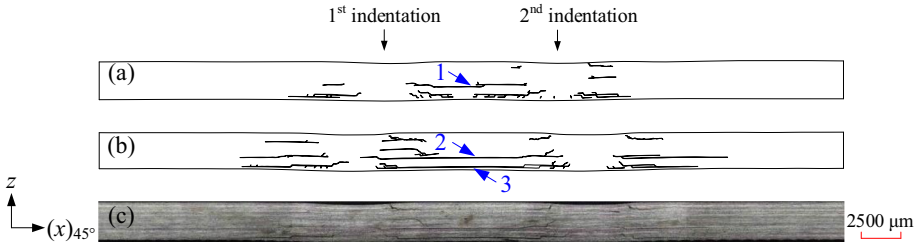

Fig. 13. Representative cross-sectional damage morphologies of the specimens: (a) with an indentation force of 3000 N, $d = d_{crit} = 12$ mm; (b) with an indentation force of 4000 N, $d = d_{crit} = 17$ mm; (c) the original damage micrograph of case (b). The left and right indentations in (b) refer to the 1st and 2nd indentations, respectively, as in (a).

Several microcracks were observed in advance of the delamination fronts; a representative photomicrograph is shown in Fig. 12. These cracks are the prelude to the indentation delamination growth [38] and are regarded as the underlying reason for the reduced effective delamination growth threshold. Intuitively, the second indentation delaminations are more likely to propagate in those crack-rich zones. However, additional research is required to determine how these cracks affects the effective delamination-growth threshold.

5.2.3. Validation of indentation force independence for delamination growth criterion

To generalise the delamination growth criterion presented in Eq. (4), further investigation is required to demonstrate its independence from a number of possible parameters, including the laminate configuration, ply interface, and indentation force. In this study, it was hypothesised that to use this criterion to predict d_{crti} for any indentation force, it must be shown that the criterion is independent of the indentation force. Applying Eq. (4) with the effective reduction to the eleventh ply interface yields

$$\left(\frac{\sigma_{13}}{\zeta S_{13}}\right)^2_{11th} = 1,\ \zeta = 0.63 \tag{5}$$

To demonstrate the validity of the delamination growth criterion, which is independent of indentation force, shown in Eq. (5), the critical loading distances for delamination link-up with indentation forces of 3000 N and 4000 N were measured in the test. The results showed that the critical loading distances related to indentation forces of 3000 N and 4000 N were approximately 12 mm and 17 mm, respectively. The corresponding representative cross-sectional damage morphologies are shown in Fig. 13, and were used to determine the interface at which delamination link-up first occurred. These specimens were sectioned along the red line, as shown in Fig. 4(c).

Fig. 13 shows that connected delaminations at the eleventh-ply interfaces of both specimens (blue numbers 1 and 2) and at the fifteenth-ply interface of the cases with an indentation force of 4000 N (blue 3). In addition, with an indentation force of 5000 N, the eleventh-ply interface was the interface at which delamination link-up first initiated (Fig. 8(d)). Therefore, the eleventh ply interface is regarded as the critical delamination link-up interface for various indentation forces. The expression for d_{crit} is

$$d_{crit} = \frac{(l_{45^\circ 11})_1 + (l_{45^\circ 11})_2}{2} \tag{6}$$

where $l_{45^\circ 11}$ is defined by Eq. (2), and the subscripts 1 and 2 refer to the first and second indentations, respectively. In this study, $(l_{45^\circ 11})_1$ and $(l_{45^\circ 11})_2$ were separately predicted by combining the delamination growth criteria shown in Eqs. (1) and (5) using the out-of-plane shear stress profiles of the eleventh ply interface.

The critical loading distance d_{crit} was determined using Eq. (6) and compared to the experimentally measured d_{crit} in Fig. 14.

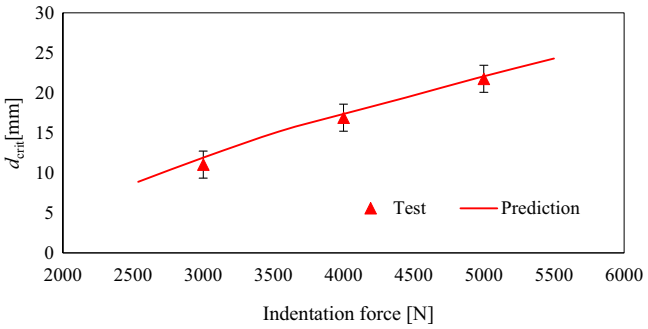

Fig. 14. Comparison of predicted and experimentally measured $d_{crit.}$

Fig. 14 strongly suggests that the delamination growth criterion shown in Eq. (5) is independent of the indentation force because the predicted and measured d_{crit} are in good agreement. This indicates that the reduction in the effective second indentation delamination growth threshold at the eleventh ply interface was constant and independent of the indentation force. Theoretically, this criterion should be applied to any of the interfaces, however, to prove the validity of this independence for each single interface, suitable damage detection techniques that can accurately differentiate between delaminations at different ply interfaces are required. Nevertheless, the research to this point indicates that when predicting the growth of the newly formed delamination in an already damaged composite laminate, a reduction in the effective delamination growth threshold should be considered.

The results also indicate that the size of the created delamination is larger due to the damage interaction, which is essentially associated with the neighbouring-damage-induced delamination threshold degradation. In this context, special attention should be paid not only to individual delaminations but also to the possibility of multiple adjacent delaminations, the combined size of which can be greater than the sum of the individual sizes.

The mutual interactions between the three basic damage modes of the composite laminates, namely matrix cracking, fibre breakage, and delamination, deserve further investigation. In particular, the fact that the size and type of new damage can be affected by existing adjacent damage must be understood. Expanding the presented approach from coupon to structural level would help create robust damage tolerant designs and allow more extensive exploration of the design space.

6. Conclusions

The delamination propagation behaviour of multidirectional CFRP composite laminates subjected to two identical indentations with different loading distances was investigated. The results indicate that delamination link-up is a distinguishing damage feature for multiple-indented laminates and that the critical loading dis-

tance for delamination link-up can be predicted using the proposed method, accounting for the damage-induced effective delamination threshold. The primary conclusion is that the effective delamination growth threshold of the newly formed delamination associated with the second indentation was reduced due to the pre-existing damages caused by the first indentation. This resulted in the longest delamination length along the delamination link-up direction in the critical case. In addition, the results suggest that the reduction in the effective delamination growth threshold at the critical delamination link-up interfaces was independent of the indentation force.

It is noteworthy that this study has the limitation that the first indentation delamination and its effects on the global critical second indentation stress profile were not considered. In the critical case, the second indentation delamination grew initially in the crack-rich zone and then connected with the first indentation delamination. This indicates that the second indentation delamination did not propagate in the delaminated ply interface and the pre-existing delamination had no directly influence on the second delamination growth. Moreover, the cohesive zone model (CZM) should be the most effective way to model the delamination damage. However, when modelling these damages, the interaction between delamination and ply damages (matrix cracking and fibre breakage) was not taken into account. To solve this problem, new modelling techniques that account for delamination-induced ply material degradation are necessary. At this point, the good agreement between the test and simulation results (Fig. 14) can effectively support the primary argument (the effective delamination growth threshold is decreased owing to the second indentation damages) of this study. Lastly, this study only investigated the delamination propagation behaviour of the composite laminates subjected to two indentations along a specific direction and interface. To generalise the conclusions, additional factors, such as stress wave, rate sensitivity of material, plate vibration, laminate configuration, delamination growth in arbitrary directions and ply interfaces, and more complex loading conditions consisting of three or more indentations, should be comprehensively considered. In particular, for the investigation of composite laminates with more than two indentations, the potential technical challenges and the modelling approach employed are comparable to those described in this study. How the pre-existing damages are affected in the subsequent indentations is the primary research question associated with the more complex loading condition, and how to significantly improve the computing efficiency is a distinct technical challenge.

Data availability

Data will be made available on request.

Declaration of Competing Interest

The authors declare that they have no known competing financial interests or personal relationships that could have appeared to influence the work reported in this paper.

Acknowledgement

The authors gratefully acknowledge the financial support from the China Scholarship Council (No. CSC201806290014).

References

[1] M. Maurya, J. Sadarang, I. Panigrahi, D. Dash, Detection of delamination in carbon fibre reinforced composite using vibration analysis and artificial neural network, Mater. Today:. Proc. 49 (2022) 517–522.
[2] Y. Cao, Z. Cao, Y. Zuo, L. Huo, J. Qiu, D. Zuo, Numerical and experimental investigation of fitting tolerance effects on damage and failure of CFRP/Ti double-lap single-bolt joints, Aerosp. Sci. Technol. 78 (2018) 461–470.
[3] Y. Cao, Z. Cao, Y. Zhao, D. Zuo, T. Tay, Damage progression and failure of single-lap thin-ply laminated composite bolted joints under quasi-static loading, Int. J. Mech. Sci. 170 (2020) 105360.
[4] D. Quan, J.L. Urdániz, A. Ivanković, Enhancing mode-I and mode-II fracture toughness of epoxy and carbon fibre reinforced epoxy composites using multi-walled carbon nanotubes, Mater. Des. 143 (2018) 81–92.
[5] D. Quan, U. Farooq, G. Zhao, C. Dransfeld, R.C. Alderliesten, Recycled carbon fibre mats for interlayer toughening of carbon fibre/epoxy composites, Mater. Des. 218 (2022) 110671.
[6] A. Wagih, P. Maimí, N. Blanco, J. Costa, A quasi-static indentation test to elucidate the sequence of damage events in low velocity impacts on composite laminates, Compos. A Appl. Sci. Manuf. 82 (2016) 180–189.
[7] M. Richardson, M. Wisheart, Review of low-velocity impact properties of composite materials, Compos. A Appl. Sci. Manuf. 27 (12) (1996) 1123–1131.
[8] S. Yashiro, K. Ogi, T. Nakamura, A. Yoshimura, Characterization of high-velocity impact damage in CFRP laminates: Part I-Experiment, Compos. A Appl. Sci. Manuf. 48 (2013) 93–100.
[9] C. Jih, C. Sun, Prediction of delamination in composite laminates subjected to low velocity impact, J. Compos. Mater. 27 (7) (1993) 684–701.
[10] M. De Moura, J. Gonçalves, A. Marques, P.T. De Castro, Modeling compression failure after low velocity impact on laminated composites using interface elements, J. Compos. Mater. 31 (15) (1997) 1462–1479.
[11] X. Sun, S. Hallett, Failure mechanisms and damage evolution of laminated composites under compression after impact (CAI): experimental and numerical study, Compos. A Appl. Sci. Manuf. 104 (2018) 41–59.
[12] W. Cantwell, J. Morton, Detection of impact damage in CFRP laminates, Compos. Struct. 3 (3–4) (1985) 241–257.
[13] Y. Aoki, H. Suemasu, T. Ishikawa, Damage propagation in CFRP laminates subjected to low velocity impact and static indentation, Adv. Compos. Mater 16 (1) (2007) 45–61.
[14] J. Zhou, B. Liao, Y. Shi, Y. Zuo, H. Tuo, L. Jia, Low-velocity impact behavior and residual tensile strength of CFRP laminates, Compos. B Eng. 161 (2019) 300–313.
[15] S. Rivallant, C. Bouvet, E. Abi Abdallah, B. Broll, J.-J. Barrau, Experimental analysis of CFRP laminates subjected to compression after impact: the role of impact-induced cracks in failure, Compos. Struct. 111 (2014) 147–157.
[16] G. Caprino, Residual strength prediction of impacted CFRP laminates, J. Compos. Mater. 18 (6) (1984) 508–518.
[17] G.J. Appleby-Thomas, P.J. Hazell, G. Dahini, On the response of two commercially-important CFRP structures to multiple ice impacts, Compos. Struct. 93 (10) (2011) 2619–2627.
[18] J. Zhou, B. Liao, Y. Shi, L. Ning, Y. Zuo, L. Jia, Experimental investigation of the double impact position effect on the mechanical behavior of low-velocity impact in CFRP laminates, Compos. B Eng. 193 (2020) 108020.
[19] B. Liao, P. Wang, J. Zheng, X. Cao, Y. Li, Q. Ma, R. Tao, D. Fang, Effect of double impact positions on the low velocity impact behaviors and damage interference mechanism for composite laminates, Compos. A Appl. Sci. Manuf. 136 (2020) 105964.
[20] B. Liao, Z. Zhang, L. Sun, J. Zhou, P. Wang, Y. Lin, W. Wu, D. Fang, Experimental investigation on the double-position impact responses and damage mechanism for Z-pinned composite laminates, Compos. Struct. 259 (2021) 113463.
[21] L.F.J. Schneider, R.R. Moraes, L.M. Cavalcante, M.A. Sinhoreti, L. Correr-Sobrinho, S. Consani, Cross-link density evaluation through softening tests: effect of ethanol concentration, Dent. Mater. 24 (2) (2008) 199–203.
[22] T.-W. Shyr, Y.-H. Pan, Impact resistance and damage characteristics of composite laminates, Compos. Struct. 62 (2) (2003) 193–203.
[23] A.J. Lesser, A.G. Filippov, Mechanisms governing the damage resistance of laminated composites subjected to low-velocity impacts, Int. J. Damage Mech 3 (4) (1994) 408–432.
[24] M. Sadighi, R.C. Alderliesten, Impact fatigue, multiple and repeated low-velocity impacts on FRP composites: a review, Compos. Struct. 297 (2022) 115962.
[25] D. Bull, S. Spearing, I. Sinclair, Investigation of the response to low velocity impact and quasi-static indentation loading of particle-toughened carbon-fibre composite materials, Compos. A Appl. Sci. Manuf. 74 (2015) 38–46.
[26] H. Kaczmarek, S. Maison, Comparative ultrasonic analysis of damage in CFRP under static indentation and low-velocity impact, Compos. Sci. Technol. 51 (1) (1994) 11–26.
[27] S.M. Lee, P. Zahuta, Instrumented impact and static indentation of composites, J. Compos. Mater. 25 (2) (1991) 204–222.
[28] L. Sutherland, C.G. Soares, The use of quasi-static testing to obtain the low-velocity impact damage resistance of marine GRP laminates, Compos. B Eng. 43 (3) (2012) 1459–1467.
[29] S.-X. Wang, L.-Z. Wu, L. Ma, Low-velocity impact and residual tensile strength analysis to carbon fiber composite laminates, Mater. Des. 31 (1) (2010) 118–125.
[30] M. Abir, T. Tay, M. Ridha, H. Lee, Modelling damage growth in composites subjected to impact and compression after impact, Compos. Struct. 168 (2017) 13–25.
[31] M. Remacha, S. Sánchez-Sáez, B. López-Romano, E. Barbero, A new device for determining the compression after impact strength in thin laminates, Compos. Struct. 127 (2015) 99–107.

[32] F. Sarasini, J. Tirillò, L. Ferrante, M. Valente, T. Valente, L. Lampani, P. Gaudenzi, S. Cioffi, S. Iannace, L. Sorrentino, Drop-weight impact behaviour of woven hybrid basalt–carbon/epoxy composites, Compos. B Eng. 59 (2014) 204–220.
[33] T. Sebaey, E. González, C. Lopes, N. Blanco, J. Costa, Damage resistance and damage tolerance of dispersed CFRP laminates: effect of ply clustering, Compos. Struct. 106 (2013) 96–103.
[34] T. Sebaey, E. González, C. Lopes, N. Blanco, P. Maimí, J. Costa, Damage resistance and damage tolerance of dispersed CFRP laminates: effect of the mismatch angle between plies, Compos. Struct. 101 (2013) 255–264.
[35] C. Santiuste, S. Sánchez-Sáez, E. Barbero, Residual flexural strength after low-velocity impact in glass/polyester composite beams, Compos. Struct. 92 (1) (2010) 25–30.
[36] Z.Y. Zhang, M.O.W. Richardson, Low velocity impact induced damage evaluation and its effect on the residual flexural properties of pultruded GRP composites, Compos. Struct. 81 (2) (2007) 195–201.
[37] H. Chenghong, L. Yubin, Z. Zuoguang, S. Zhijie, Impact damage modes and residual flexural properties of composites beam, J. Reinf. Plast. Compos. 27 (11) (2008) 1163–1175.
[38] L. Huo, C. Kassapoglou, R.C. Alderliesten, A criterion for predicting delamination growth in composite laminates, Mater. Des. 223 (2022) 111160.
[39] Delta-tech, DT120 versatile high toughness epoxy matrix, 2015.
[40] R. Rodi, R.C. Alderliesten, R. Benedictus, Crack-tip behavior in fiber/metal laminates by means of digital-image correlation, J. Aircr. 47 (5) (2010) 1636–1646.
[41] L. Huo, R.C. Alderliesten, M. Sadighi, Delamination initiation in fully clamped rectangular CFRP laminates subjected to out-of-plane quasi-static indentation loading, Compos. Struct. 303 (2023) 116316.
[42] C.-S. Lee, J.-H. Kim, S.-K. Kim, D.-M. Ryu, J.-M. Lee, Initial and progressive failure analyses for composite laminates using Puck failure criterion and damage-coupled finite element method, Compos. Struct. 121 (2015) 406–419.
[43] K. Kodagali, Progressive Failure Analysis of Composite Materials using the Puck Failure Criteria, University of South Carolina, 2017. Master thesis),.